Nuclear Engineering and Technology 55 (2023) 850–860

Contents lists available at ScienceDirect

Nuclear Engineering and Technology

journal homepage: www.elsevier.com/locate/net

Original Article

Energy-saving optimization on active disturbance rejection decoupling multivariable control

Da-Min Ding [a, b, f], Hai-Ma Yang [a, c, f, *], Jin Liu [d], Da-Wei Zhang [a], Xiao-Hui Jiang [e]

[a] School of Optical-Electrical and Computer Engineering, University of Shanghai for Science and Technology, Shanghai, 200093, China
[b] Rehabilitation Engineering and Technology Institute, University of Shanghai for Science and Technology, Shanghai, 200093, China
[c] Key Laboratory of Space Active Opto-electronics Technology, Chinese Academy of Sciences, Shanghai, 200083, China
[d] School of Electronic and Electrical Engineering, Shanghai University of Engineering Science, Shanghai, 201620, China
[e] School of Mechanical Engineering, University of Shanghai for Science and Technology, Shanghai, 200093, China
[f] 516 Jungong Road, Yangpu District, Shanghai 200093, China

ARTICLE INFO

Article history:
Received 23 May 2022
Received in revised form
13 October 2022
Accepted 20 November 2022
Available online 24 November 2022

Keywords:
LOCA
ADRC
Multiple input multiple output
Multivariable
Energy saving

ABSTRACT

An industrial control process multiple-input multiple-output (MIMO) coupled system is analyzed in this study as an example of a Loss of Coolant Accident (LOCA) simulation system. Ordinary control algorithms can complete the steady state of the control system and even reduce the response time to some extent, but the entire system still consumes a large amount of energy after reaching the steady state. So a multivariable decoupled energy-saving control method is proposed, and a novel energy-saving function (economic function, Eco-Function) is specially designed based on the active disturbance rejection control algorithm. Simulations and LOCA simulation system tests show that the Eco-function algorithm can cope with the uncertainty of the multivariable system's internal parameters and external disturbances, and it can save up to 67% of energy consumption in maintaining the parameter steady state.

1. Introduction

Most industrial control systems are MIMO systems, and many of them are multi-parameter coupled systems. The study of decoupling control of such complex time-delay systems has become an important topic in current process control research [1]. With the rapid development of manufacturing, MIMO systems have become increasingly widely used in industrial applications, and MIMO control has received much attention in the past decades. Decoupling control used in the nuclear power industry is an important part [2].

In recent years there have been some novel intelligent decoupling methodologies [3,4]. [5] developed a practical multivariable control method, consisting of inverted decoupling and a decentralized active disturbance rejection controller (ADRC). Strong robustness is achieved with negligible computation and simple forms of the decoupler and controller, and the disturbance rejection is markedly accelerated. An identification method for first-order and second-order delay systems is studied based on the least-squares method [6]. For the coupling of multivariable systems, the inverted decoupling method is used to decouple the plant. And then an active disturbance rejection controller is designed for the decoupled delay subsystem. Given the coupling relationship between the radial degrees of freedom of the magnetic bearing system, a method based on sliding mode active disturbance rejection decoupling control was proposed [7]. To ensure the fast dynamic response of the system, sliding mode control was introduced into the nonlinear state error feedback control law, and sliding mode active disturbance rejection controllers of their respective degrees were designed. An effective inverse-solving method for the variable high-order matrix is presented in Ref. [8], and this method is a LU matrix decomposition approach based on the Gaussian elimination procedure.

At present, many scholars have conducted research and explored multivariable coupled control [9–11], and have achieved many results, and emphasized that the effectiveness of model-based multivariable controllers depends on the quality of the model used.

* Corresponding author. School of Optical-Electrical and Computer Engineering, University of Shanghai for Science and Technology, Shanghai, 200093, China.
E-mail addresses: dmding@ieee.org (D.-M. Ding), snowyhm@sina.com (H.-M. Yang).

https://doi.org/10.1016/j.net.2022.11.013

In the field of the nuclear power industry, there are some specific scenarios, such as the loss of coolant accident (LOCA) test system, which simulates the loss of coolant accident environment in nuclear power and maintains the dual-parameter balance of temperature and pressure required by the environment, a stress analysis of an AP1000 reactor containment is performed in a LOCA [12]. 50% hot leg break CSR1000 LOCA is analyzed in Ref. [13].

In the study by Wang, GY, Yan, YK et al., an experimental natural circulation facility was built by scaling down from a typical PWR-type SMR for the analysis of LOCA and loss of heat sink accident (LOHS) [14]. Kim MG et al. discussed the development of future intelligent nuclear power plant control systems and improved the economical operation mode of nuclear power plants by analyzing the LOCA characteristics of large pressurized water reactors (PWRs) and small modular reactors (SMRs) [15]. Simulating LOCA experiments requires a large amount of energy. In particular, a test may last for several months, and the supply of hot steam is generated by the combustion of liquefied petroleum gas, which is expensive.

In this paper, we analyze LOCA cabin as a MIMO coupled system and model it, and propose a control method suitable for multi-parameter coupled systems based on ADRC. An energy-saving module containing the energy-saving function Eco-Function is designed to reduce the input and output synchronously and save energy. Finally, the simulation and experiment are carried out to analyze the control effect and energy consumption.

The contributions of this paper are as follows:

(1) We analyze the stabilization process of the multivariate system and create a decoupled model;
(2) For this model, an effective ADRC-based control method is designed;
(3) In this method, an Eco-Function is innovatively designed, which can reduce energy consumption.

The rest of this paper is organized as follows: In Section VI, we present related work. In Section III, we present ADRC and Linear ADRC theory. In Section IV, the LOCA test system is analyzed and modeled, an algorithm based on ADRC is designed, and an Eco-Function is innovatively designed for this algorithm. The experiments are detailed in Section V. Finally, we present our concluding observations in Section VI.

2. Related works

There are many studies on various methods of controlling coupled MIMO systems in industrial processes. M. M. Machado [16] provided research and development of a multivariable control system for temperature and liquid levels consisting of three tanks, a MIMO system with two inputs (hot and cold water), and two outputs (level and temperature process variables). Sergio Fragoso [17] used decoupling controllers to improve variable-speed variable-pitch wind turbine performance. Pavel Navrátil [18] combined the original inverted decoupling with disturbance rejection to control the two-variable controlled plant of a quadruple tank. These methods are limited by the fact that the number of inputs needs to be equal to the number of outputs, and the amount of computation is large.

Shubham Khandelwal [19] proposed a centralized PI control design methodology, and the off-diagonal (OD) controllers in the centralized PI control framework are designed using the DPI controllers and the process steady-state gain. ChunyanWang [20] presents a composite decoupling control method, which consists of a neural network inverse system and a robust controller. The results of the simulation and vehicle test show that the proposed decoupling controller has excellent decoupling performance, which can transform the multivariable system into several single-input and single-output systems. Sudeshna Dasgupta [21] presented a decoupling controller for a multivariable time-delay system, using IMC structure in an innovative way to control the distillation column. Cuiping Pu [22] regards the coupling between channels as disturbance by decentralized ADRC, they adopted the multivariable extended state observer and combined the inverse decoupling design and ADRC to achieve better decoupling control. These methods do not solve the energy loss problem well.

The Eco-Function algorithm proposed in this paper can be easily integrated with other MIMO control systems, Shibo provides an ADRC-based multivariable decoupling control method to control a small pressurized water reactor (PWR) pressurizer [23], which can be regarded as a simplified version of our proposed methods by removing Eco-Function and changing LADRC back to ADRC.

Unlike the above methods, we have one more closed-loop system than the general MIMO control method and reduce the energy consumption of the system by introducing Eco-Function. Moreover, if the energy consumption is negligible, we can directly set the parameter k_{eco} in Eco-Function to 0.

3. Background

Active Disturbances Rejection Controler (ADRC) is a summary based on PID control theory and modern control theory [24]. It draws the essence of PID core control theory and modern control theory and combines nonlinear characteristics with PID [24]. The reason we use an ADRC-based control algorithm instead of PID-based is that PID, which passively eliminates errors based on error feedback, lags behind the influence of disturbances, and may cause system oscillations due to excessive control force. The integral link set to eliminate the residual error will make the phase angle of the system lag. Moreover, the integral link does not have an obvious inhibitory effect on the change disturbance and is easily polluted by noise. In multivariable system control, there will be more noise than in univariate systems due to system coupling. Therefore, it is necessary to suppress the disturbance in a targeted manner. Active Disturbances Rejection Controller is mainly composed of a Tracking differentiator (TD), Extended state observer (ESO), Nonlinear PD (NPD), and disturbance compensation process. The structure of the n-order ADRC is shown in Fig. 1, where v is the system input, y is the system output, e is the error, u is the control quantity, z is the state estimation signal, and w is the disturbance quantity.

Han Jingqing [24] derived the fastest synthesis function ***fhan*** for ADRC. Zhiqiang Gao linearized the extended state observer ESO of nonlinear ADRC [25], related its parameters to the observer bandwidth, simplified the ESO to LESO, adopted a simple PD (Proportion

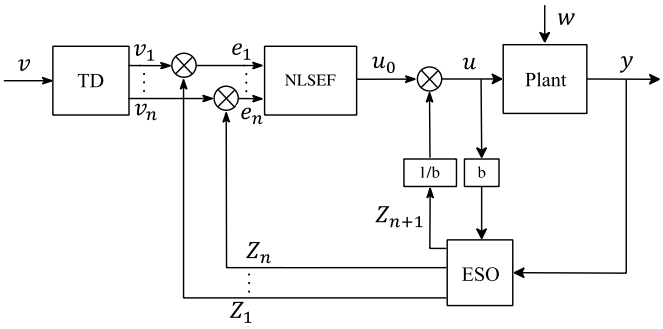

Fig. 1. Schematic diagram of ADRC structure.
Note: ADRC Control Algorithm by Ref. [24].

Differentiation) control combination, and combined k_p, k_d with the controller bandwidth. k_p is the proportional gain, and k_d is the differential gain. The parameter setting of the entire controller is simplified, and the work of linear ADRC (LADRC) is completed. Its basic structure diagram is shown in Fig. 2:

In Fig. 2, u_d is the system disturbance, z_1 and z_2 are the LESO estimation of y and the differential estimation of y, and z_3 is the estimation of u_d by LESO.

4. Methodology

When controlling a multi-parameter model of a multivariable equilibrium system, it is usually only necessary to control the system to maintain its corresponding equilibrium stable state. The LOCA experimental cabin can be abstractly understood as the model shown in Fig. 3:

Fig. 3 shows a simplified model with two parameters that need to be satisfied, namely the resultant force F and the upper and lower equilibrium position S of the marker. We can see from Fig. 3 that the confrontation between f_1 and f_2 mainly affects S, while the confrontation between f_1, f_2, and f_3 mainly affects F.

After reaching the stable state from the initial 0 states, the time is very short. It is necessary to increase f_1, f_2, and decrease f_3 first. When the acceleration a reaches the desired value and the position indicated by the pointer marker reaches the desired value, we want to reduce f_1, f_2, and f_3, and at the same time, the system maintains the current stable state, so that the energy consumption of the whole system is reduced.

Fig. 4 shows the LOCA experimental Cabin system. The volume of the hot steam tank and the compressed air tank is much larger than that of the LOCA experimental cabin. This control requires the provision of large cabins to store high-temperature steam (usually above 400 °C [26]) and low-temperature air, respectively, to supply the experimental cabin to conduct simulated LOCA experiments. During the month after reaching stability, the experiment required the consumption of a large amount of hot steam. The cost of producing high-temperature steam is huge, therefore, reducing steam consumption has become a very important issue.

In the process of the LOCA experimental cabin test, the temperature in the cabin is required to rise directly from room temperature to above 150 °C in just 1 s, and the pressure in the cabin rises from standard atmospheric pressure to above 0.45 MPa. This temperature and pressure need to be maintained for a month or more [27]. The above indicators CPR1000 requires a temperature of 156 °C and pressure of 0.56 MPa [28]; AP1000 requires a temperature of 220 °C and a pressure of 0.35–0.4 MPa [28], and HuaLong No. 1 requires a temperature of 150 °C and a required pressure of 0.47 MPa.

Fig. 5 shows the specific requirements for LOCA identification in Standards for Design and Construction of Electrical Equipment of Pressurized Water Reactor Nuclear Power Plant Nuclear Island

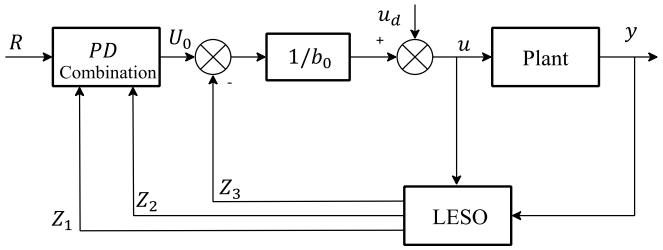

Fig. 2. Schematic diagram of Linear ADRC structure.
Note: Linear ADRC Control Algorithm by Ref. [25].

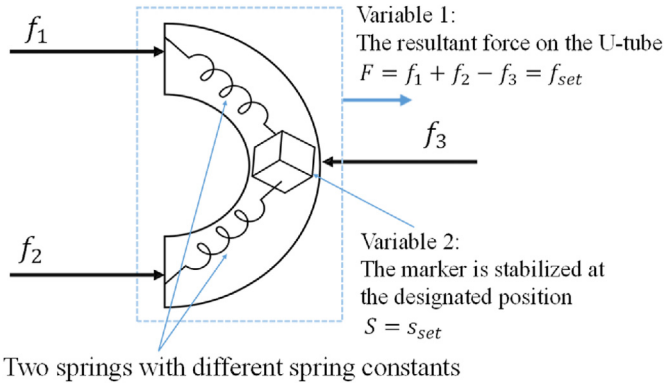

Fig. 3. Schematic diagram of a two-parameter coupled system.
Note: Equivalent mechanical model analyzed in this manuscript.

Electrical Equipment, which is divided into 8 stages. Let's take this curve as an example. The process of area 1 in Fig. 5 is as follows:

(1) Thermal shock process: within 1 s, the temperature in the experimental cabin should be raised from the previous room temperature to 156 °C, and the pressure should be raised from the previous 1-atmosphere pressure to 0.56 MPa. This test step usually requires opening the electric regulating actuator valve in advance and suddenly opening the pneumatic flange ball valve to complete.

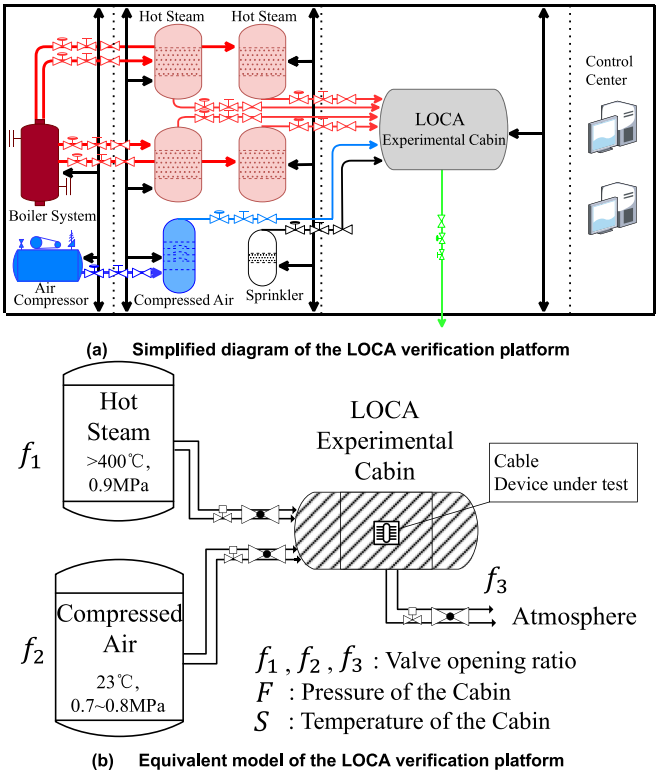

Fig. 4. LOCA experimental cabin system ((a) The structure of the system, (b) Schematic diagram of the working principle of the experimental cabin).
Note: The overall structure of the LOCA experimental cabin system is shown in the figure. The system is supplied with hot steam and normal temperature air by a boiler system and an air compressor. The hot steam enters four huge hot steam tanks, and the compressed air enters a huge cold air tank. When the experiment starts, these gases will be fed into the experimental cabin.

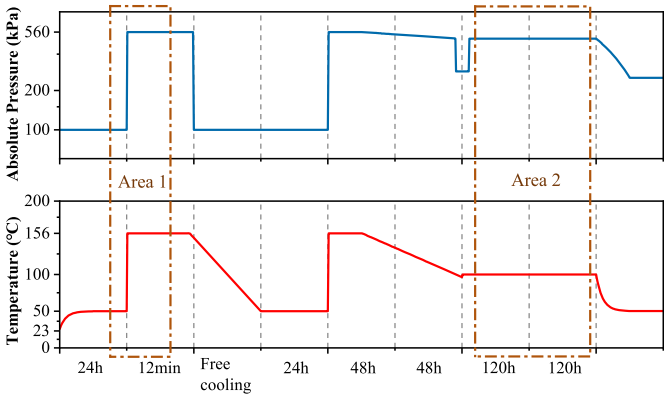

Fig. 5. French standard LOCA identification curve.
Note: The specific requirements for LOCA identification, also the environment in which the LOCA accident occurred.

(2) Equilibrium process: In the next 12min, keep the temperature and pressure at this step value.

The above thermal shock step process requires opening all the steam inlet valves, air inlet valves, and exhaust valves in an instant. The temperature of the LOCA experimental cabin in Area2 is 120 °C and the pressure is about 0.5 MPa.

In the process of Area 2, we mainly analyze the process of keeping the pressure and temperature at high temperature and high pressure. The process requires precise control of steam valves, air valves, and exhaust valves to maintain stability. The generation of hot steam requires the combustion of liquefied petroleum gas, there are problems of large energy consumption, the system runs for a long time, and the volume of the steam storage compartment is limited. How to reduce steam and air consumption is the main research problem of this paper.

4.1. LOCA experimental cabin analysis and modeling

Taking the LOCA experimental cabin as the analysis object, as shown in Fig. 6:

Fig. 6(a) is the external shape of the experimental cabin, and Fig. 6(b) is the internal display. Hot steam and normal temperature compressed air are input into the cabin, and there is an exhaust valve at the bottom to discharge the gas. The interior of the experimental cabin is a large hollow cavity, and the interior needs to simulate the high temperature and high-pressure environment generated when the LOCA accident occurs. As a controlled object, its system structure diagram can be simplified in Fig. 7:

In Fig. 7, the experimental cabin has three input quantities,

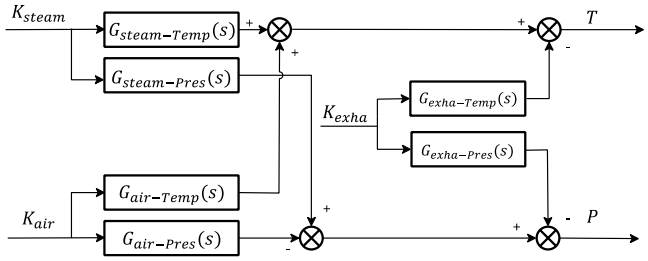

Fig. 7. Schematic diagram of the LOCA experimental cabin as the controlled object.
Note: The experimental cabin has three input quantities, which are the opening degree K_{steam} of the hot steam inlet valve, the opening degree K_{air} of the air inlet valve, and the opening degree K_{exha} of the exhaust valve. The three valves are controlled in real-time. The output variables are the temperature T and pressure P of the LOCA experimental cabin.

which are the opening degree K_{steam} of the hot steam inlet valve, the opening degree K_{air} of the air inlet valve, and the opening degree K_{exha} of the exhaust valve.

The three valves are controlled in real-time by the controller. The output variables are the temperature T and pressure P in the experimental cabin. When the inlet air valve is open, its effect on pressure is positive and its effect on temperature is reversed; when the inlet steam valve is open, its effect on pressure is positive, and the effect on temperature is positive; when the exhaust valve is opened, its effect on pressure is reversed, and the effect on temperature is also reversed. It can be seen that the flexible control of the three valves can theoretically stabilize the temperature and pressure in the experimental cabin.

Let $\Delta T = T_{cabin} - T_{set}$, $\Delta P = P_{cabin} - P_{set}$, there is:

$$\frac{dT_{cabin}}{dt} = f_T(K_{steam}, K_{air}, K_{exha}, \Delta T) \tag{1}$$

$$\frac{dP_{cabin}}{dt} = f_P(K_{steam}, K_{air}, K_{exha}, \Delta P) \tag{2}$$

$f_T(K_{steam}, K_{air}, K_{exha}, \Delta T)$ in Eq. (1) can be broken down into the effect of three valves on temperature. In the analysis of this model, the effect of exhaust gas on the temperature is very small and can be ignored or regarded as an external disturbance [24], and only the effect of the inlet steam valve K_{steam} and the air inlet valve K_{air} on the temperature of the experimental cabin is studied. $\frac{1}{\omega_{T-steam}}$ is the electromechanical time constant and $\frac{k_{T-steam}}{\omega_{T-steam}}$ is the gain to the temperature, there is:

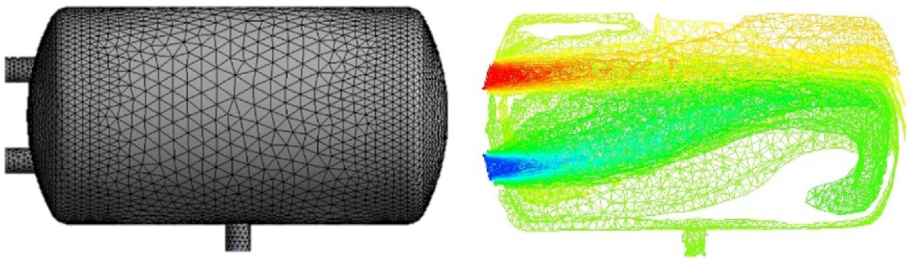

(a) The shape of the experimental cabin **(b) The interior of the experimental cabin**

Fig. 6. Schematic diagram of the shape and working state of the LOCA experimental cabin ((a) The shape of the experimental cabin. (b) The interior of the experimental cabin).
Note: The shape and working internal state of the LOCA experimental cabin, the red area represents hot steam, the blue area represents normal temperature air, and their pressure is higher than 0.7 MPa. (For interpretation of the references to colour in this figure legend, the reader is referred to the Web version of this article.)

$$\frac{d^2T_{cabin}}{dt^2} = -\omega_{T-steam} \bullet \frac{dT_{cabin}}{dt} - k_{T-steam} \bullet T_{cabin} + k_{T-steam} \bullet K_{steam} - \omega_{T-air} \bullet \frac{dT_{cabin}}{dt} - k_{T-air} \bullet T_{cabin} + k_{T-air} \bullet K_{air} \tag{3}$$

$f_P(K_{steam}, K_{air}, K_{exha}, \Delta P)$ can be decomposed into the effect of three valves on pressure. $\frac{1}{\omega_{T-steam}}$ is the electromechanical time constant and $\frac{k_{T-steam}}{\omega_{T-steam}}$ is the gain to the pressure, there is:

$$\frac{d^2P_{cabin}}{dt^2} = -\omega_{P-steam} \bullet \frac{dP_{cabin}}{dt} - k_{P-steam} \bullet P_{cabin} + k_{P-steam} \bullet K_{steam} - \omega_{P-air} \bullet \frac{dP_{cabin}}{dt} - k_{P-air} \bullet P_{cabin} + k_{P-air} \bullet K_{air} - \omega_{P-exha} \bullet \frac{dP_{cabin}}{dt} - k_{P-exha} \bullet P_{cabin} + k_{P-exha} \bullet K_{exha} \tag{4}$$

The transfer function matrix of the LOCA experimental cabin can be expressed as:

$$G_{ij}(s) = \begin{bmatrix} G_{steam-Temp}(s) & G_{air-Temp}(s) & 0 \\ G_{steam-Pres}(s) & G_{air-Pres}(s) & G_{exha-Pres}(s) \end{bmatrix} \tag{5}$$

Then its mathematical model is:

$$\begin{bmatrix} y_{Temp} \\ y_{Pres} \end{bmatrix} = \begin{bmatrix} \frac{k_{T-steam}}{s(s+\omega_{T-steam})} & -\frac{k_{T-air}}{s(s+\omega_{T-air})} & 0 \\ \frac{k_{P-steam}}{s(s+\omega_{P-steam})} & \frac{k_{P-air}}{s(s+\omega_{P-air})} & -\frac{k_{P-exha}}{s(s+\omega_{P-exha})} \end{bmatrix} \times \begin{bmatrix} u_{steam} \\ u_{air} \\ u_{exha} \end{bmatrix} \tag{6}$$

After reaching the equilibrium and stable state, if all the steam inlet valves, air inlet valves, and exhaust valves are closed, the temperature in the experimental cabin will still decrease slowly due to heat conduction, and the pressure will also decrease due to the relationship of temperature. Therefore, after reaching equilibrium in the peak pulling process, closing all valves immediately cannot complete the subsequent maintenance of temperature and pressure.

4.2. Control algorithm

We add a compensation amount at the valves of the steam and air intake to maintain the intake state and prevent the phenomenon that the pressure cannot reach the target value. With the compensation amount at the intake end, it can be seen that the intake air is always open, and we need to find a balance between the intake steam and the intake air. The traditional two-parameter control method based on LADRC is shown in Fig. 8 below:

As shown in Fig. 8, the LADRC output value U_1 is the ratio of the steam valve to the air valve, the sum of which equals 100%. When the temperature T_{cabin} of the experimental cabin is lower than T_{set}, the first set of LADRC will increase the opening of the steam valve, increase the supply of steam, and reduce the supply of air, at this time $U_1 > 0.5$; when the temperature of the experimental cabin T_{cabin} is higher than T_{set}, the first set of LADRC will reduce the opening of the steam valve, reduce the supply of steam, and increase the supply of air, at this time $U_1 < 0.5$.

The above method has realized the control of the dual

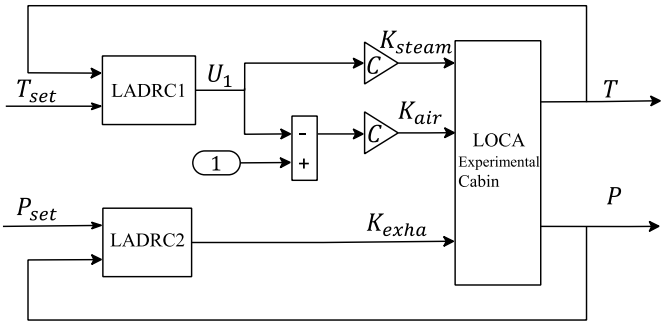

Fig. 8. Traditional control method based on LADRC.
Note: This is a traditional control method based on linear ADRC, without the innovative point Eco-Function of this manuscript.

parameters of temperature and pressure of the experimental cabin. After the two parameters reach a steady-state, the coupled system needs a method to reduce energy consumption, which is mainly the consumption of hot steam. The modified method is shown in Fig. 9:

As shown in Fig. 9, the fixed value compensation amount in Fig. 8 is changed to a dynamically variable compensation amount. The compensation amount consists of two parts, one part is the intake valve opening calculated by the second set of LADRC, which is opposite to the exhaust opening; the other part is the compensation amount calculated by the compensation amount calculation module, which adds the third set of LADRC and Eco-Function. The coexistence of these two parts can not only prevent the intake valve from closing prematurely when the temperature reaches the expectation and the pressure is insufficient; it also prevents the intake valve from closing prematurely when the pressure reaches the expectation and the temperature is insufficient.

In the beginning, T_{cabin} is lower than T_{set}, and the first set of LADRC turns up the steam valve, open to the maximum 100%, at this time the air valve and exhaust valve are both 0;

1) After a while, the temperature T_{cabin} reaches the desired temperature T_{set}, while the pressure P_{cabin} has not yet reached the desired pressure P_{set}. The opening ratio of the steam valve will decrease, and the opening ratio of the air valve will begin to rise. At this time, the temperature of the experimental cabin T_{cabin} is stable near the expected temperature T_{set}, and the absolute value of the temperature error $|\Delta T|$ will be within a small range;

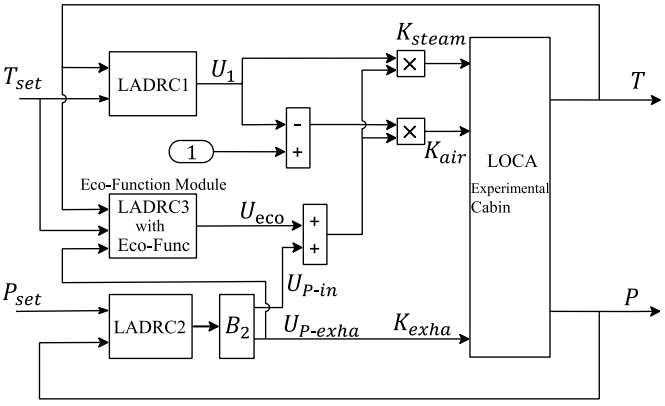

Fig. 9. Design of the control method with the addition of the energy-saving algorithm Eco-Function.
Note: This is the control method based on the linear ADRC and Eco-Function designed in this manuscript. It has one more closed-loop system and Eco-Function than the traditional method.

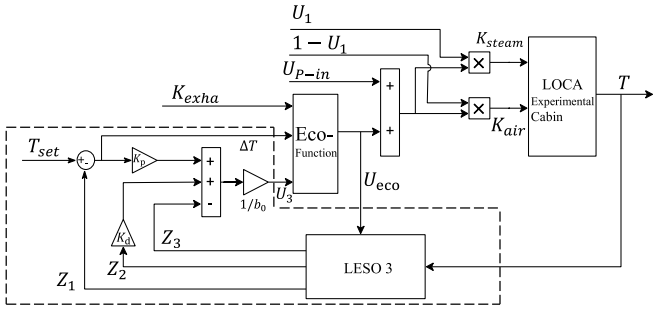

Fig. 10. Schematic diagram of the energy-saving algorithm structure.
Note: Here are the details of the closed-loop system and Eco-Function.

2) Due to the existence of the compensation amount, the steam valve and the air valve will not be closed, but continue to be input to the LOCA experimental cabin and mixed into the experimental cabin in a corresponding proportion until the pressure P_{cabin} of the experimental cabin reaches the expected value P_{set}.
3) In the later stage, the steam valve opening K_{steam}, the air valve opening K_{air}, and the exhaust opening K_{exha} tend to be stable.

In the process of maintaining stable temperature and pressure, the compensation amount calculation will reduce its compensation value, and the second set of LADRC calculates the exhaust amount that is not closed. Eventually, the system reaches temperature and pressure stability, and the intake valve opening is reduced to the minimum required to maintain multivariate stability, there are:

$$\begin{cases} y_{steam} = U_1 = \dfrac{K_{steam}}{K_{steam}+K_{air}} \times 100\% \\ y_{air} = 1-U_1 = \dfrac{K_{air}}{K_{steam}+K_{air}} \times 100\% \\ K_{steam}+K_{air} = U_{eco}+U_{P-in} \end{cases} \tag{7}$$

The total amount of input gas calculated by the second set of LADRC and $\boldsymbol{B_2}$ is:

$$U_{P-in} = \begin{cases} U_P;\ if\ U_P \geq 0 \\ 0;\ if\ U_P < 0 \end{cases} \tag{8}$$

The total number of exhaust valves is:

$$U_{P-exha} = \begin{cases} 0;\ if\ U_P \geq 0 \\ -U_P;\ if\ U_P < 0 \end{cases} \tag{9}$$

In the intake valve, the relationship between hot steam and compressed air is:

$$\begin{cases} K_{steam} = U_1 \times (U_{eco}+U_{P-in}) \\ K_{air} = (1-U_1) \times (U_{eco}+U_{P-in}) \\ K_{exha} = U_{P-exha} \end{cases} \tag{10}$$

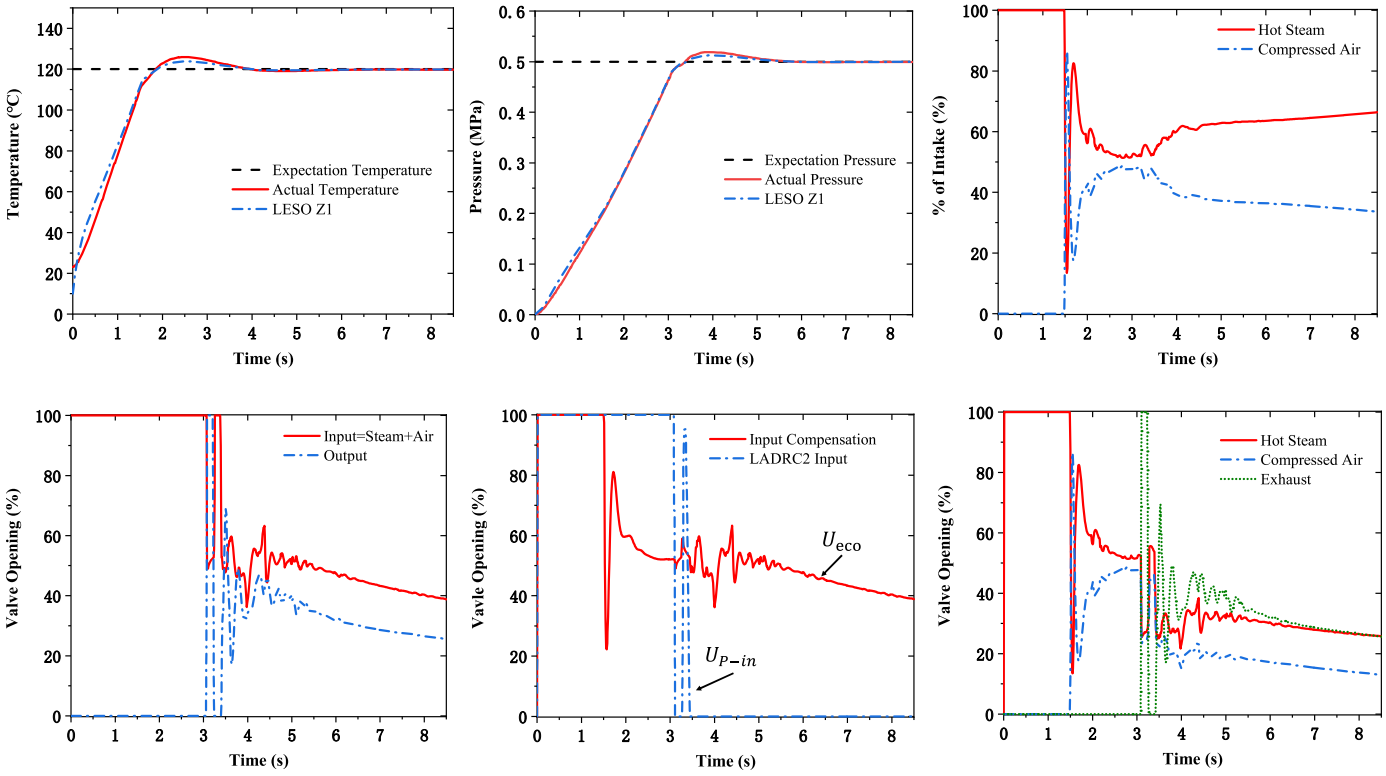

Fig. 11. Performance of the LOCA experimental cabin((a) Temperature of the LOCA experimental cabin, (b) Pressure of the LOCA experimental cabin, (c) Valve opening curves for hot steam and compressed air, (d) Valve opening curve for input ($\boldsymbol{K_{in}} = \boldsymbol{K_{steam}} + \boldsymbol{K_{air}}$) and output, (e) Input compensation $\boldsymbol{U_{eco}}$ and original input (without compensation) $\boldsymbol{U_{P-in}}$ curves by the second set of LADRC, (f) Curves for hot steam, compressed air, and exhaust valves).
Note: (a) Temperature of the LOCA experimental cabin, (b) Pressure of the LOCA experimental cabin, (c) Valve opening curves for hot steam and compressed air, (d) Valve opening curve for input ($K_{in} = K_{steam} + K_{air}$) and output, (e) Input compensation U_{eco} and original input (without compensation) U_{P-in} curves by the second set of LADRC, (f) Curves for hot steam, compressed air, and exhaust valves.
It can be seen that the new algorithm can complete the valve control well, and finally close the small steam valve.

4.3. Energy-saving algorithm and Eco-Function

The control algorithm with the third set of LADRC and energy-saving functions controls the valve of the steam and the compressed air to decrease after the LOCA cabin system reaches the desired temperature and pressure, to achieve the purpose of saving energy.

The structure of the third set of LADRC and Eco-Function is shown in Fig. 10. The input expected temperature T_{set} is compared with the output Z_1 of LESO, and Z_1 participates in the operation of the controller as negative feedback. The second half is similar to LADRC. The intake compensation amount U_{eco} is calculated by the Eco-Function:

$$U_{eco} = |U_3| - \frac{K_{exha}}{k \cdot e^{|\Delta t|}} \tag{11}$$

Where U_3 is the output of the first half of the LADRC in Fig. 10, and K_{exha} in Eco-Function is equal to the exhaust valve opening U_{P-exha}, which is calculated by the second set of LADRC in Fig. 9, k is the speed parameter, which can change the change speed of the entire compensation amount. Denote k_{eco} as $^1/_k$, then Eco-Function can be written as:

$$U_{eco} = |U_3| - k_{eco} \cdot K_{exha} \cdot e^{-|\Delta t|} \tag{12}$$

Eco-Function(12) shows:

1) When the temperature T_{cabin} in the experimental cabin is far from the expected temperature T_{set}, $|\Delta t| \gg 0$, $U_{eco} \approx |U_3|$;
2) When the temperature T_{cabin} in the experimental cabin is close to the expected temperature T_{set}, $\Delta t \approx 0$, two situations can be analyzed at this time. When the pressure P_{cabin} of the experimental cabin is far from the desired pressure P_{set}, the second set of LADRC in Fig. 12 will automatically adjust the intake and exhaust, and the opening is large enough to adjust the pressure error $\Delta p = 0$. When the pressure P_{cabin} of the experimental cabin is close to the desired pressure P_{set}, $U_{eco} \approx |U_3| - k_{eco} \cdot U_{exha}$, which can be approximated as:

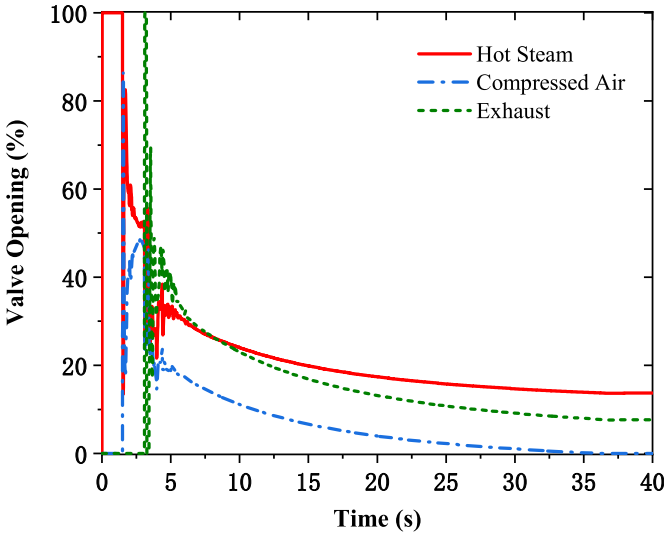

Fig. 12. Curves for hot steam, compressed air, and exhaust valves (The difference from Fig. 11(f) is that the time is 40s).
Note: Change the abscissa: time of Fig. 11(f) from 8 s to 40 s. It can be seen that the hot steam and exhaust gas are reduced to a certain extent and become stable. This is the minimum incoming hot steam value to combat system leakage and heat dissipation.

$$\frac{dU_{eco}}{dt} = -k_{eco} \cdot \frac{dK_{exha}}{dt} \tag{13}$$

Where k_{eco} is the speed parameter, which is a constant.

It can be seen from Eco-Function (12) that when the compensation amount U_{eco} decreases, that is, the intake air amount $K_{in} = K_{steam} + K_{air}$ begins to decrease, and the exhaust valve K_{exha} begins to increase. However, in the control system of Fig. 10, according to the output U_2 of the second set of LADRC, when the intake air amount K_{in} decreases, to maintain the experimental cabin pressure P_{cabin} equal to the desired pressure P_{set}, the exhaust gas amount K_{exha} needs to start to decrease. Therefore, the intake air amount K_{in} will reach an equilibrium position with the exhaust air amount K_{exha}. This stable state fully considers the heat loss due to heat conduction and the gas escape due to cracks in the experimental cabin at room temperature. When the experimental cabin is an ideal cavity, that is, no heat loss occurs, and the cavity is well sealed, then the intake air valve K_{in} and the exhaust air valve K_{exha} will eventually reach 0. At this time, there is no steam or air input into the experimental cabin, the cabin temperature T_{cabin}, and pressure P_{cabin} are expected values.

5. Experiments

5.1. Experimental details

System identification is carried out for a LOCA experimental system in Shanghai, China, and transfer functions are constructed respectively.

The model of the LOCA experimental cabin can be expressed by (6) as:

$$\begin{bmatrix} T_{cabin} \\ P_{cabin} \end{bmatrix} = \begin{bmatrix} \frac{k_{T-steam}}{s(s+\omega_{T-steam})} & \frac{-k_{T-air}}{s(s+\omega_{T-air})} & 0 \\ \frac{k_{P-steam}}{s(s+\omega_{P-steam})} & \frac{k_{P-air}}{s(s+\omega_{P-air})} & \frac{-k_{P-exha}}{s(s+\omega_{P-exha})} \end{bmatrix} \times \begin{bmatrix} u_{steam} \\ u_{air} \\ u_{exha} \end{bmatrix} = \begin{bmatrix} \frac{336}{s(s+47.6)} & \frac{-282}{s(s+43.2)} & 0 \\ \frac{0.71}{s(s+47.6)} & \frac{0.99}{s(s+43.2)} & \frac{-1.1}{s(s+41.4)} \end{bmatrix} \begin{bmatrix} u_{steam} \\ u_{air} \\ u_{exha} \end{bmatrix} \tag{14}$$

To simulate the process of natural heat dissipation and cooling, we add a differential equation to the controlled object as (15):

$$\frac{dy}{dt} = -(y - 23) \times 0.001 \tag{15}$$

Where y represents the temperature, the default room temperature is 23 °C, so there is this offset in the formula. 0.001 is used as the gain value to make the control effect intuitively. There will not be such serious heat conduction in cooling and air leakage. Due to good protective measures, the real LOCA cabin will not have such serious heat conduction.

After increasing the heat conduction and heat dissipation effect of the experimental cabin as (15), the temperature control curve is shown in Fig. 11(a). Similarly, the pressure control curve is shown in Fig. 11(b). The temperature T_{cabin} and pressure P_{cabin} finally reached their target values.

Fig. 11(c) shows the ratio of hot steam to air. Fig. 11(d) shows the relationship between the input valve and the exhaust valve in the experimental cabin after increasing the heat dissipation. It can be seen that the proportion of hot steam increases, but the overall

intake air volume decreases.

Fig. 11(e) shows the relationship between the input compensation U_{eco} and the initial intake U_{P-in} calculated by the second set of LADRC. Fig. 11(f) shows the curves for hot steam, compressed air, and exhaust valves, it is evident that the consumption of both hot steam and compressed air is decreasing

Fig. 12 shows that when the temperature and pressure of the LOCA experimental cabin are stable, the hot steam valve is finally maintained at 13.71%, and the air valve dropped to 0%, the exhaust valve remained at 7.69%. The opening of the intake valve is larger than that of the exhaust valve because the exhaust pipe is thicker than the steam intake pipe. This hot steam opening value of 13.71% is the minimum value that will maintain the LOCA cabin temperature at the desired value.

The comparison with and without Eco-Function is shown in Fig. 13. It shows the effect of a control algorithm with an energy-saving function Eco-Function on the hot steam and compressed air input to the LOCA experimental cabin. Here is a simple quantification of energy savings. For steam consumption, there are:

$$V = \int_0^t k_{steam} \bullet k \bullet \Delta P \bullet \frac{v}{100} dt \tag{16}$$

where V is the total cost, k_{steam} is the steam valve opening, $k \bullet \Delta P$ is the speed of steam entering the LOCA experimental cabin, and k is related to the thickness of the pipe. v is the production cost per cubic meter of steam, calculated based on the consumption of 8 kg of liquefied gas when a 20 m^3 steam warehouse is filled, the diameter of the pipeline is 9 cm, and the price of a liquefied petroleum gas (LPG) tank with 48 kg is 71.43 dollars. Assuming the hot steam is an ideal gas:

Fig. 14 shows the energy consumption curves with and without Eco-Function. It can be seen that the new method with Eco-Function consumes less energy than the traditional method after the two-parameter balance of temperature and pressure is completed. It is foreseeable that the LOCA test will save a lot of money in the thermal insulation link of more than 20 days.

Table 1 shows the relevant data from Fig. 14. The data shows that the energy consumption of the two algorithms is not much different when the temperature and pressure reach the expected values. However, in the later stage of process control, the control algorithm with Eco-Function can significantly save economic expenses to maintain a stable state. Even with uncontrollable heat dissipation, it still reduces the cost of LPG by more than 67% compared with the traditional algorithm.

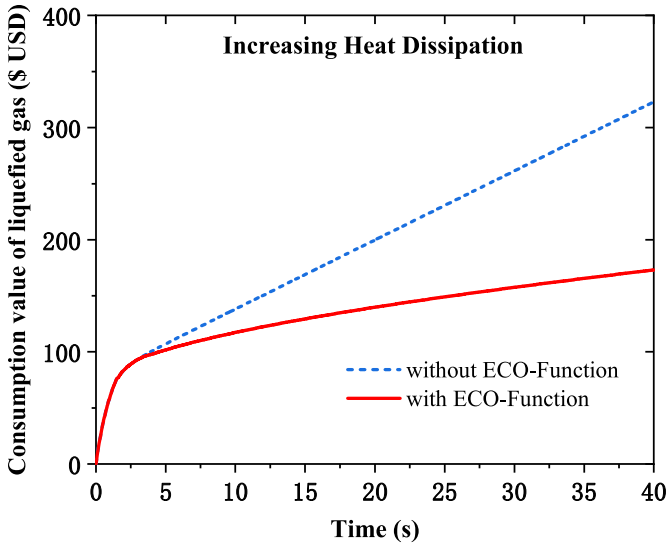

Fig. 14. The effect of Eco-function on energy consumption.
Note: The price of LPG consumed by different algorithms, it can be seen that Eco can save this part of consumption from Fig. 14.

5.2. Anti-disturbance verification

For the LOCA experimental cabin, the main disturbance to the system is the effect of the closed-loop control of one parameter on another parameter. For example, in the temperature closed-loop, the pressure in the experimental cabin will increase when the incoming steam heats up. At the 20th s, the simulation adds a steam inlet with a maximum opening of 10% and a positive sine wave disturbance with a duration of 5s. The changes in temperature and pressure are shown in Fig. 15:

Fig. 15(a) and (b) show that the fluctuations in temperature and pressure are relatively small. Fig. 15(d) shows that the Eco-Function does not hinder the control in the algorithm when the disturbance increases. In addition, we also simulated the experiment of using the traditional control method of Fig. 8 without the Eco-Function, and the results are shown in Table 2:

In Table 2, the overshoots of the control algorithm with Eco-Function added are not much different from the control method without Eco-Function, which shows that the noise immunity of the control algorithm with Eco-Function is not weaker than that without Eco-Function.

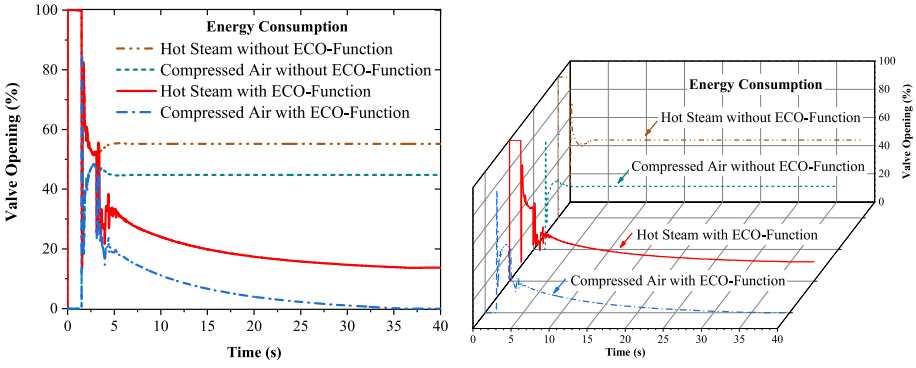

Fig. 13. Effect of Eco-function on the consumption of hot steam and air((a) Curves displayed in 2D, (b) Curves displayed in 2D).
Note: Effect of Eco-function on the consumption of hot steam and air that shown in 2D and 3D figure. It can be seen that with Eco-Function, the consumption of hot steam drops significantly.

Table 1
Cost Calculation of LPG Consumption in LOCA Test ($ US dollars).

	No heat dissipation 40s cost	Increasing heat dissipation 40s cost	Increasing heat dissipation 7s cost	Increasing heat dissipation 7s–40s cost
method without Eco-Function	28.933	32.289	11.967	20.322
method with Eco-Function	11.152	17.317	10.859	6.458

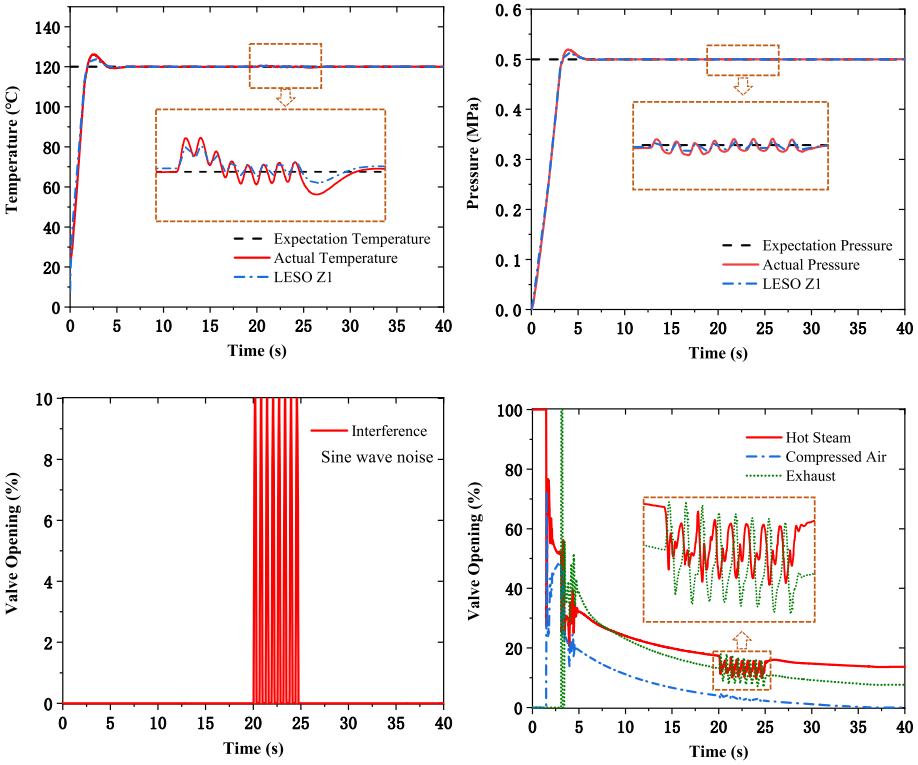

Fig. 15. Anti-disturbance verification experimental results((a) Temperature of the LOCA Cabin with details, (b) Pressure of the LOCA Cabin with details, (c) Interference sine wave noise disturbance (20s–25s), (d) Curves for hot steam, compressed air, and exhaust valves with details.).
Note: Fig. 15(a)(b)(c)(d) shows the anti-disturbance verification experimental results. (a) The temperature of the LOCA Cabin with details, (b) The pressure of the LOCA Cabin with details, (c) Interference sine wave noise disturbance (20s–25s), (d) Curves for hot steam, compressed air, and exhaust valves with details.
It can be seen from Fig. 15 that the new algorithm has good anti-interference performance.

Table 2
Influence of disturbance on control performance.

	temperature overshoot	pressure overshoot
method without Eco-Function	0.65 °C	0.0004 MPa
method with Eco-Function	0.63°C	0.0004 MPa

5.3. Robustness verification

Change the gains of $G_{steam-Pres}(s)$, $G_{air-Pres}(s)$, and $G_{exha-Pres}(s)$ in the transfer function to 0.91, 0.79, and 0.9. The control parameters of LADRC and Eco-Function are both unchanged. The expected temperature is set to a step value of 120 °C, and the expected

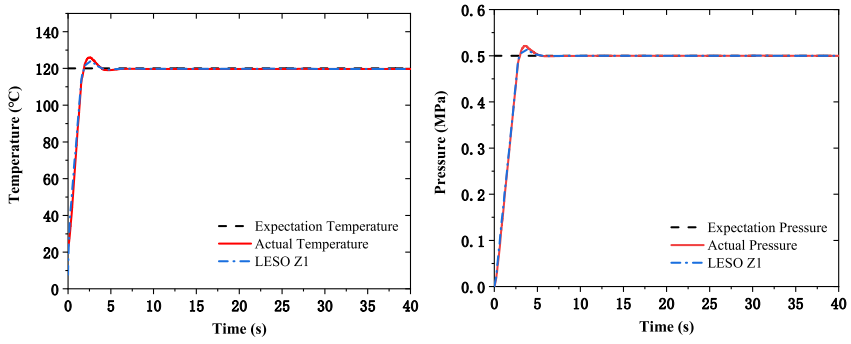

(a) Temperature of the LOCA experimental cabin (b) Pressure of the LOCA experimental cabin

Fig. 16. Robustness verification experimental results((a) Temperature of the LOCA experimental cabin, (b) Pressure of the LOCA experimental cabin).
Note: Fig. 16(a)(b) shows the robustness verification experimental results. (a) Temperature of the LOCA experimental cabin, (b) Pressure of the LOCA experimental cabin. The comparison of Fig. 16(a)(b) and Fig. 11(a)(b) shows that the change of the gain has little influence on the control algorithm, indicating that the system has good robustness.

Fig. 17. A LOCA experimental cabin in Shanghai, China (partial).
Note: Here is a photo we took of the LOCA experimental cabin in Shanghai, China, where the Eco-Function algorithm has been applied.

pressure is set to 0.5 MPa. The changes in temperature T_{cabin} and pressure P_{cabin} are shown in Fig. 16:

The comparison of Figs. 16 and 11(a)(b) shows that the change of the gain has little influence on the control algorithm, indicating that the system has good robustness.

Fig. 17 shows a LOCA experimental system in Shanghai, where the Eco-Function algorithm has been applied.

5.4. Discussion

In this paper, we propose a multi-parameter closed-loop energy algorithm based on LADRC, in which an innovative energy-saving function is designed. This method can be applied to a multi-parameter closed-loop control system and can reduce the energy consumption of the system, which has good economic benefits. The experimental environment of the LOCA experimental cabin needs to consume a huge amount of energy, so in the stabilization link, we will pay more attention to energy saving.

We can predict that there are some experimental objects whose energy consumption is not very sensitive, or there is a relatively generous but also upper limit energy consumption range. We will continue to study the energy-saving algorithm in-depth so that it can choose an optimal point between better stable performance and limited energy consumption, that is, k_{eco} of Eco-Function (12). Source codes of this paper are available on GitHub(ericddm/LOCA-Eco-Function).

6. Conclusion

In some typical multi-parameter closed-loop decoupling control, it is a common problem to save energy as much as possible after the system reaches stability. Aiming at this problem, this paper proposes a control method with good immunity and robustness, which can well complete the parameter decoupling and can save and maintain steady-state energy. Among them, energy-saving modules and energy-saving function Eco-Function are innovatively designed to save energy. The Eco-Function algorithm has a large degree of freedom and only needs to adjust one parameter, which is relatively easy to apply and promote. Experiments show that the algorithm can solve the problem well.

Declaration of competing interest

The authors declare that they have no known competing financial interests or personal relationships that could have appeared to influence the work reported in this paper.

Acknowledgments

This work is partially support by the Open Research Fund of Key Laboratory of Space Active Optical-Electro Technology, CAS: No. 2021ZDKF4, and Action Plan of Technological Innovation of Shanghai City Science and Technology Commission: 21S31904200, 22S31903700.

References

[1] L. Liu, S. Tian, D. Xue, T. Zhang, Y. Chen, S. Zhang, A review of industrial MIMO decoupling control, Int. J. Control Autom. Syst. 17 (5) (2019) 1246–1254, https://doi.org/10.1007/s12555-018-0367-4.
[2] A. Nuerlan, P. Wang, J. Wan, F. Zhao, Decoupling header steam pressure control strategy in multi-reactor and multi-load nuclear power plant, Prog. Nucl. Energy 118 (2020), 103073, https://doi.org/10.1016/j.pnucene.2019.103073.
[3] T. Chekari, R. Mansouri, M. Bettayeb, IMC-PID fractional order filter multi-loop controller design for multivariable systems based on two degrees of freedom control scheme, Int. J. Control Autom. Syst. 16 (2) (2018) 689–701, https://doi.org/10.1007/s12555-016-0699-x.
[4] M. Kim, T.-Y. Kuc, H. Kim, J.S. Lee, Adaptive iterative learning controller with input learning technique for a class of uncertain MIMO nonlinear systems, Int. J. Control Autom. Syst. 15 (1) (2017) 315–328, https://doi.org/10.1007/s12555-016-0049-z.
[5] L. Sun, J. Dong, D. Li, K.Y. Lee, A practical multivariable control approach based on inverted decoupling and decentralized active disturbance rejection control, Ind. Eng. Chem. Res. 55 (7) (2016) 2008–2019, https://doi.org/10.1021/acs.iecr.5b03738.
[6] Y. Cheng, Z. Chen, M. Sun, Q. Sun, Multivariable inverted decoupling active disturbance rejection control and its application to a distillation column process, Acta Autom. Sin. 43 (6) (2017) 1080–1088, https://doi.org/10.16383/j.aas.2017.c170137.
[7] B. li, L. Zeng, P. Zhang, Z. Zhu, Active magnetic suspension bearing sliding mode active anti-jamming decoupling control, Electr. Mach. Control/Dianji Yu Kongzhi Xuebao 25 (7) (2021).
[8] B. Sui, Z. Huang, Nonlinear mimo decoupling adrc control method based on real-time variable inverse matrix solution, Fire Control Command Control 46 (12) (2021) 8, https://doi.org/10.3969/j.issn.1002-0640.2021.12.007.
[9] S. Misra, M. Darby, S. Panjwani, M. Nikolaou, Design of experiments for control-relevant multivariable model identification: an overview of some basic recent developments, Processes 5 (3) (2017) 42, https://doi.org/10.3390/pr5030042.
[10] G. Scaglia, E. Serrano, A. Rosales, P. Albertos, Tracking control design in nonlinear multivariable systems: robotic applications, Math. Probl Eng. 2019 (2019), https://doi.org/10.1155/2019/8643515.
[11] A.M.d. Almeida, M.K. Lenzi, E.K. Lenzi, A survey of fractional order calculus applications of multiple-input, multiple-output (mimo) process control, Fractal. Fractional. 4 (2) (2020) 22, https://doi.org/10.3390/fractalfract4020022.
[12] S. Sheykhi, S. Talebi, M. Soroush, E. Masoumi, Thermal-hydraulic and stress analysis of ap1000 reactor containment during loca in dry cooling mode, Nucl. Sci. Tech. 28 (6) (2017) 1–13, https://doi.org/10.1007/s41365-017-0233-8.
[13] J. Chen, T. Zhou, L. Liu, X. Fang, Analysis on LOCA for CSR1000, Ann. Nucl. Energy 110 (2017) 903–908, https://doi.org/10.1016/j.anucene.2017.07.026.
[14] G. Wang, Y. Yan, S. Shi, X. Yang, M. Ishii, Experimental study on accident transients and flow instabilities in a PWR-type small modular reactor, Prog. Nucl. Energy 104 (2018) 242–250, https://doi.org/10.1016/j.pnucene.2017.10.004.
[15] M.-G. Kim, J.I. Lee, Implication of LOCA characteristics of large PWR and SMR for future development of intelligent nuclear power plant control system, Ann. Nucl. Energy 127 (2019) 237–247, https://doi.org/10.1016/j.anucene.2018.12.010.
[16] M. Machado, A. Carvalho, M. Santos, J. De Carvalho, Case study: level and temperature multivariable control and design via arduino through control loop decoupling, in: 2018 19th International Carpathian Control Conference (ICCC), IEEE, 2018, pp. 247–252, https://doi.org/10.1109/CarpathianCC.2018.8399636.
[17] S. Fragoso, J. Garrido, F. Vázquez, F. Morilla, Comparative analysis of decoupling control methodologies and h∞ multivariable robust control for variable-speed, variable-pitch wind turbines: application to a lab-scale wind turbine, Sustainability 9 (5) (2017) 713, https://doi.org/10.3390/su9050713.
[18] P. Navrátil, L. Pekař, R. Matuš, Control of a multivariable system using optimal control pairs: a quadruple-tank process, IEEE Access 8 (2019) 2537–2563,

https://doi.org/10.1109/ACCESS.2019.2962302.
[19] S. Khandelwal, S. Aldhandi, K.P. Detroja, Centralized control with decoupling approach for large scale multivariable processes, in: TENCON 2019-2019 IEEE Region 10 Conference (TENCON), IEEE, 2019, pp. 2633–2638, https://doi.org/10.1109/TENCON.2019.8929297.
[20] C. Wang, W. Zhao, Z. Luan, Q. Gao, K. Deng, Decoupling control of vehicle chassis system based on neural network inverse system, Mech. Syst. Signal Process. 106 (2018) 176–197, https://doi.org/10.1016/j.ymssp.2017.12.032.
[21] S. Dasgupta, S. Sadhu, Decoupling controller design for a multivariable time delay system, in: 2020 IEEE 1st International Conference for Convergence in Engineering (ICCE), IEEE, 2020, pp. 189–194, https://doi.org/10.1109/ICCE50343.2020.9290724.
[22] C. Pu, J. Ren, A. Yu, Decoupling control of distillation column based on active disturbance rejection control, in: 2021 3rd International Conference on Applied Machine Learning (ICAML), IEEE, 2021, pp. 477–481, https://doi.org/10.1109/ICAML54311.2021.00106.
[23] B. Shi, D. Li, W. Guo, Y. Zhang, Study on multivariable decoupling control of small PWR pressurizer based on active disturbance rejection control, Nucl. Power Eng. 42 (5) (2021) 143–148, https://doi.org/10.13832/j.jnpe.2021.05.0143.
[24] J. Han, From PID to active disturbance rejection control, IEEE Trans. Ind. Electron. 56 (3) (2009) 900–906, https://doi.org/10.1109/TIE.2008.2011621.
[25] Z. Gao, Scaling and bandwidth-parameterization based controller tuning, Proc. Am. Control Conf. 6 (2006) 4989–4996, https://doi.org/10.1109/ACC.2003.1242516.
[26] Z. Wang, J. Yan, Y. Lin, T. Fang, J. Ma, Study on failure mechanism of pre-stressed concrete containments following a loss of coolant accident, Eng. Struct. 202 (2020), 109860, https://doi.org/10.1016/j.engstruct.2019.109860.
[27] L. Wang, W. Tian, P. Zhang, K. Zhang, Y. Zhang, M. Wang, Y. Xiang, S. Qiu, G. Su, H. Chang, Development and applicability analyses of ads-4 entrainment model in large advanced PWR, Nucl. Eng. Des. 356 (2020), 110379, https://doi.org/10.1016/j.nucengdes.2019.110379.
[28] Y.Q. Li, H.J. Chang, Z.S. Ye, F.F. Fang, Y. Shi, K. Yang, M.T. Cui, Analyses of acme integral test results on cap1400 small-break loss-of-coolant-accident transient, Prog. Nucl. Energy 88 (2016) 375–397, https://doi.org/10.1016/j.pnucene.2016.01.012.